

MEEG and AT-DGNN: Improving EEG Emotion Recognition with Music Introducing and Graph-based Learning

1st Minghao Xiao, 1st Zhengxi Zhu, 3rd Bin Jiang*, 4th Meixia Qu, 5th Wenyu Wang

School of Mechanical, Electrical & Information Engineering, Shandong University, Weihai, China

Email: {202237585, 202200800179}@mail.sdu.edu.cn, {jiangbin, mxqu, hochi}@sdu.edu.cn

Abstract—Neuropsychological research highlights the essential role of coordinated activities across brain regions during cognitive tasks. This study expands the existing EEG datasets by constructing the MEEG dataset, a multi-modal compilation of music-induced electroencephalogram (EEG) recordings, and further investigates the brain network topology during emotional responses to music. The MEEG dataset, capturing emotional responses to various musical stimuli across different valence and arousal levels, enables an in-depth analysis of brainwave patterns within musical contexts. We introduce the Attention-based Temporal Learner with Dynamic Graph Neural Network (AT-DGNN), a novel framework for EEG emotion recognition. By integrating an attention mechanism with a dynamic graph neural network (DGNN), the AT-DGNN model captures complex local and global EEG dynamics, demonstrating superior performance with accuracy of 83.74% in arousal and 86.01% in valence, outperforming current state-of-the-art (SOTA) methods. Comparative analyses with traditional datasets like DEAP underscore our model’s effectiveness, highlighting the potential of music as a potent emotional stimulus. This study advances graph-based learning techniques in brain-computer interfaces (BCI), significantly enhancing the precision of EEG-based emotion recognition and deepening our understanding of cognitive functions in various brain regions. The source code and dataset are accessible at <https://github.com/xmh1011/AT-DGNN>.

Index Terms—electroencephalogram, emotion recognition, dynamic graph neural networks.

I. INTRODUCTION

Emotion, a complex physiological and psychological phenomenon, plays a critical role in interpreting genuine reactions to daily interactions [1]. In 1980, Russell introduced the dimensional models of emotion, with the Valence-Arousal (VA) model being particularly noteworthy [2]. The model conceptualizes emotions within a continuous dimensional space, providing a framework that allows for a more nuanced quantification of emotional states.

BCI technology decodes EEG signals, which reflect cortical voltage fluctuations, into commands for external devices, enhancing human-machine interaction [3, 4]. This technology involves preprocessing, feature extraction, and classification stages, translating thoughts into actionable commands. Due to their objectivity, high temporal resolution, affordability, and rapid acquisition, EEG signals are indispensable for emotion recognition and neuroscience research [5, 6].

In 2011, Koelstra et al. established the DEAP dataset, which consists of physiological signals, such as EEG, elicited

by emotional responses to musical videos [7]. Subsequently, Zheng et al. introduced the SEED dataset in 2015, comprising well-annotated EEG signals induced by cinematic stimuli, with data collected from multiple subjects [8]. These datasets have significantly contributed to the advancement of computational models for emotion analysis. Over the past decades, a variety of machine learning and signal processing techniques have been applied to emotion recognition based on physiological data.

Recent advances in deep learning have significantly impacted EEG signal processing. In 2018, Lawhern et al. proposed EEGNet, a compact convolutional neural network (CNN) tailored for EEG analysis [9]. Subsequent developments by Schirrmeister et al. further refined EEG decoding capabilities using deep CNN architectures, introducing sophisticated visualization tools [10]. The adoption of temporal convolutional networks (TCNs) has introduced robust alternatives for real-time BCI applications. Notably, in 2020, Ingolfsson et al. developed EEG-TCNet, which demonstrated superior accuracy in motor imagery tasks, suggesting that TCNs could outperform traditional methods in specific BCI contexts [11]. This assertion was corroborated by Musallam et al., who demonstrated the versatility and efficiency of TCNs in complex BCI tasks, particularly through the integration of TCNs in motor imagery classification [12].

All the aforementioned research treated EEG signals primarily as two-dimensional time-series data, with dimensions corresponding to channels and time [13]. Here, channels denote EEG electrodes, positioned on the scalp using the 10-20 system, as prescribed by the International Federation of Clinical Neurophysiology, to capture neural activity from distinct brain regions [3]. More recently, a paradigm shift has occurred with EEG data now being conceptualized as graphs, representing the electrodes’ two-dimensional arrangement on the scalp [14]. In this model, raw data or extracted features from each electrode augment this spatial framework by adding a third dimension [15].

In 2023, Ding et al. introduced the Local-Global-Graph network (LGGNet) to process EEG data in an image-like format, improving classification performance [16]. However, LGGNet’s single-layer graph neural network (GNN) struggles to capture the dynamic features of EEG signals. Additionally, popular EEG datasets like DEAP and SEED primarily use

video stimuli, limiting the study of the relationship between music, emotions, and EEG signals. In contrast, EEG datasets and research using other types of stimuli are relatively scarce.

To address shortcomings in emotion recognition research, we create the MEEG dataset, a multi-modal EEG emotion dataset in the DEAP format with music-induced emotional states to enhance ecological validity. We improve the LGGNet architecture by integrating an attention mechanism and using a multi-layer dynamic graph neural network, significantly boosting classification accuracy on the MEEG dataset. This innovative approach allows for a more nuanced examination of brain function interconnections via graph-based learning.

The contributions of our study are threefold and can be summarized as follows:

- 1) We establish the MEEG dataset, a multi-modal EEG emotion dataset in the DEAP format, enhanced with various types of music to effectively induce emotional states. Experimental results show that the MEEG dataset outperforms the video-stimuli-based DEAP dataset in emotion induction, effectively enhancing model ACC and F1 scores.
- 2) We propose the AT-DGNN framework for exploring connections within and between different functional areas of the brain. By integrating an attention mechanism and employing DGNN, the LGGNet architecture is significantly enhanced for emotion recognition.
- 3) We compare the performance of the proposed method with CNN, TCN, and GNN-based SOTA methods on the MEEG dataset. Extensive ablation experiments are conducted to better understand AT-DGNN.

II. RELATED WORK

A. Multi-head Attention Mechanism

EEG data is inherently complex, characterized by temporal dependencies and discrete features. Utilizing multiple attention heads allows us to capture a diverse range of temporal patterns and dependencies, effectively identifying key temporal features. In this module, the attention block consists of a multi-head attention (MHA) layer with several self-attention heads.

Each self-attention head comprises three fundamental components: queries Q , keys K , and values V . These elements facilitate the computation of attention scores that influence the weighting of the values. The process begins with normalizing the input X_w via a layer normalization (*LayerNorm*):

$$\begin{cases} q_{ht} = W^Q \text{LayerNorm}(X_{w,t}) \\ k_{ht} = W^K \text{LayerNorm}(X_{w,t}) \\ v_{ht} = W^V \text{LayerNorm}(X_{w,t}) \end{cases} \quad (1)$$

Here, q_{ht} , k_{ht} , and v_{ht} denote the queries, keys, and values at time t for head h , derived from the normalized input. The matrices W^Q , W^K , and W^V belong to $\mathbb{R}^{d \times d_H}$, where d_H represents the dimension of each attention head. This normalization facilitates the efficient computation of attention scores.

The attention context vector c_{ht} for each head is computed as a weighted sum of the values, with weights $\alpha_{htt'}$ determined by the scaled dot-product attention mechanism. The alignment scores $e_{htt'}$ are calculated as:

$$e_{htt'} = \frac{(q_{ht})^T k_{ht'}}{\sqrt{d_H}} \quad (2)$$

Here, t' denotes the different time steps considered. The softmax function converts these scores into a probability distribution, reflecting the importance of each value vector:

$$c_{ht} = \sum_{t'} \alpha_{htt'} v_{ht'} \quad (3)$$

where $\alpha_{htt'}$ represents the normalized alignment scores, indicating the importance of each value vector $v_{ht'}$ in forming the context vector c_{ht} for time step t . This context vector c_{ht} captures the most relevant information from the values, highlighting key features at each time step.

B. Graph Neural Networks

GNNs represent a significant advancement in the domain of neural networks, designed explicitly to process graph-structured data. Unlike CNNs, GNNs excel in capturing the intricate relationships and dependencies among nodes within a graph through processes of aggregation and propagation of information across local neighbors [17]. A typical graph is denoted as $G = (V, E)$, where V symbolizes the set of nodes and E the set of edges. Each node $v_i \in V$ and edge $e_{ij} = (v_i, v_j) \in E$ can be respectively associated with a node and an edge in the graph. The adjacency matrix A is configured as an $n \times n$ matrix where $A_{ij} = 1$ if $e_{ij} \in E$ and $A_{ij} = 0$ otherwise. Node attributes are represented by X , where $X \in \mathbb{R}^{n \times d}$, with each $x_i \in \mathbb{R}^d$ denoting the feature vector of node v_i .

DGNNs extend the capabilities of GNNs to address dynamic or time-evolving graph-structured data. In DGNNs, a graph at any given time t is represented as $G_t = (V_t, E_t)$, with its corresponding adjacency matrix A_t . This matrix changes dynamically as nodes and edges are added or removed over time. Node features at time t are likewise dynamic, represented as X_t with each row $x_{t,i} \in \mathbb{R}^d$ embodying the evolving feature set of node v_i .

The computational heart of DGNNs lies in the dynamic update rules, where node representations $h_{t,i}$ are recurrently updated based on the temporal graph structure. A prevalent approach involves the temporal graph attention mechanism, where the new node states are computed as:

$$h_{t,i}^{(k+1)} = \sigma \left(\sum_{j \in \mathcal{N}(v_i)} \alpha_{t,ij}^{(k)} W^{(k)} h_{t,j}^{(k)} + b^{(k)} \right) \quad (4)$$

Here, $\mathcal{N}(v_i)$ represents the neighbors of node v_i , $\alpha_{t,ij}^{(k)}$ are the attention coefficients indicating the significance of the features of neighbor j to node i , and $W^{(k)}$ and $b^{(k)}$ are trainable parameters of the k -th layer, with $\sigma(\cdot)$ being a non-linear activation function.

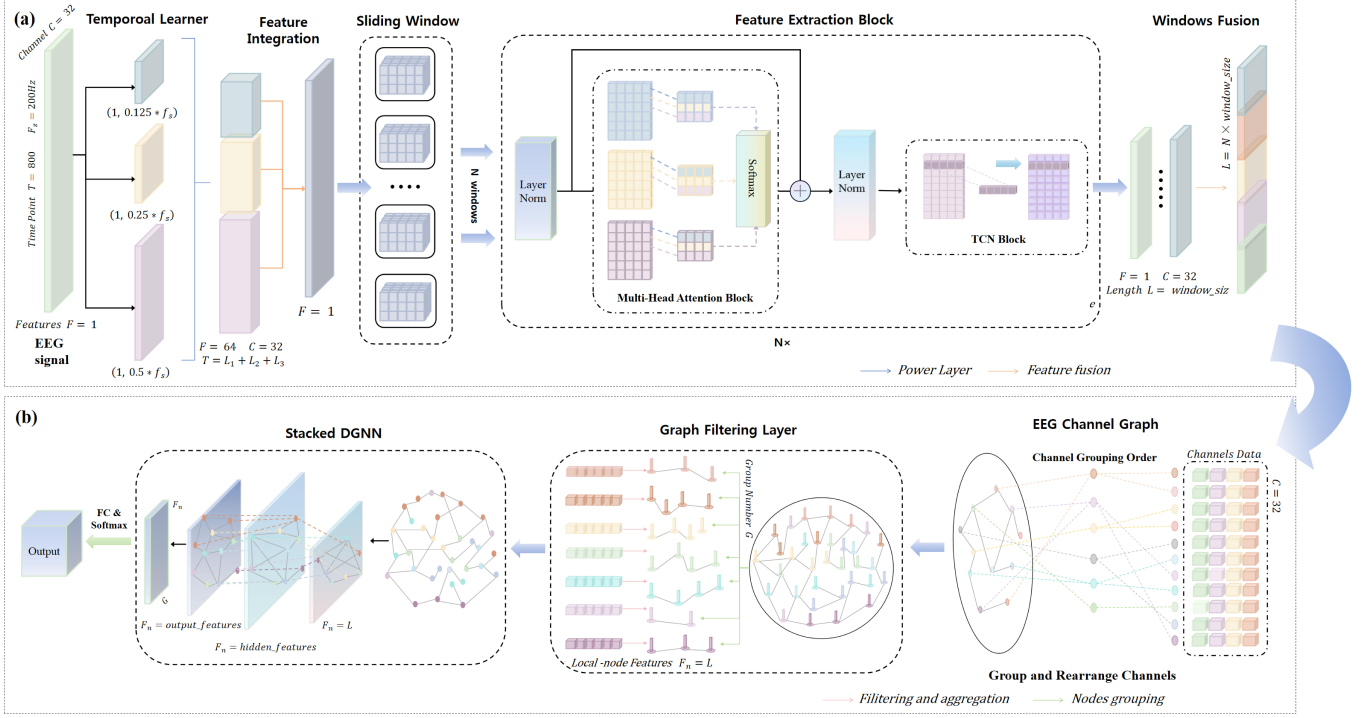


Fig. 1: Structure of AT-DGNN. The AT-DGNN model comprises two core modules: a feature extraction module (a) and a dynamic graph neural network learning module (b). The feature extraction module consists of a temporal learner, a multi-head attention mechanism, and a temporal convolution module. These components effectively leverage local features of EEG signals through a sliding window technique, thereby enhancing the model's capacity to dynamically extract complex temporal patterns in EEG signals. In the graph-based learning module, the model initially employs local filtering layers to segment and filter features from specific brain regions. Subsequently, the architecture employs three layers of stacked dynamic graph convolutions to capture complex interactions among different brain regions. This structure enhances the AT-DGNN's capacity for integrating temporal features effectively.

C. Graph Neural Networks for EEG

In 2019, Song et al. [18] first introduced a novel DGCNN specifically for multichannel EEG emotion recognition, employing an adjacency matrix to dynamically model EEG channel relationships and enhance feature discrimination. This method proved to be superior to existing approaches. Subsequently, advancements in GNNs have been increasingly applied to emotion recognition. On the SEED dataset, Bao et al. [19] integrated a multi-layer GNN with a style-reconfigurable CNN, while Asadzadeh et al. [20] further improved the DGCNN by incorporating Bayesian signal recovery techniques, both achieving enhanced performance. For the DEAP dataset, Zhao et al. [21] developed coherence-based node clustering and multi-pooling techniques for GCNs. Additionally, Zhang et al. [22] enhanced GCN feature extraction by using Granger causality analysis and differential entropy to construct more informative connectivity matrices.

III. METHODOLOGY

In this section, we introduce the detailed architecture of AT-DGNN from the three aspects of data preprocessing, feature extraction and graph-based learning in turn, and the overall structure of AT-DGNN is shown in Fig. 1.

A. EEG Data Preprocessing

The initial sampling rate of the MEEG dataset is 1000 Hz. To align with standard EEG datasets typically sampled at 128 Hz or 200 Hz, and to mitigate issues such as high artifact noise and overlapping interference signals, the data are downsampled to 200 Hz. This preprocessing phase involves the use of a band-pass filter with a range of 1 to 50 Hz to enhance the signal quality by minimizing interference. Subsequently, the EEG signals are segmented into five distinct frequency bands for feature extraction: Delta (1-4 Hz), Theta (4-8 Hz), Alpha (8-14 Hz), Beta (14-31 Hz), and Gamma (31-50 Hz) [23].

B. Feature Extraction

1) *Temporal Learner*: A temporal learner layer employing multiscale 1D temporal kernels (T kernels) is used to directly extract dynamic temporal representations from EEG data $X_i \in \mathbb{R}^{E \times T}$, where E denotes the number of EEG electrodes, and T is the sample length. These kernels obviate the need for manually extracted features. The i th-kernel's length (S_T^i), dictated by the sampling frequency (f_s) of EEG data and scaling coefficients (α^i), is given by [24]:

$$S_T^i = (1, \alpha^i \cdot f_s), \quad i \in [1, 2, 3] \quad (5)$$

EEG data processed through these layers yield dynamic time-frequency representations. An average pooling (*AvgPool*) layer, acting as a window function, calculates the averaged power across shorter segments. The logarithmic activation as described by [10] is applied to improve the performance. The output from each layer i , denoted as Z_{temp}^i , is formulated as:

$$Z_{temp}^i = \Phi_{log}(\text{AvgPool}(\Phi_{sqr}(\mathcal{F}_{Conv1-D}(X_i, S_T^i)))) \quad (6)$$

Here, $\Phi_{log}(\cdot)$ is the logarithmic activation function, $\Phi_{sqr}(\cdot)$ represents the square function, and $\mathcal{F}_{Conv1-D}(\cdot)$ signifies the 1D convolution operation.

The outputs across all kernels are concatenated along the feature dimension to yield the final output of the temporal learner layer Z_T :

$$Z_T = f_{bn}(Z_{temp}^1, Z_{temp}^2, Z_{temp}^3) \quad (7)$$

where $f_{bn}(\cdot)$ denotes the batch normalization operation.

2) *Sliding Window Segmentation*: Following the temporal learner, a convolution-based sliding window technique as [25] is applied to segment the EEG time series X into multiple windows. This method integrates sliding window segmentation with convolutional operations, significantly reducing computational overhead by allowing convolutions to be executed once across all windows. This approach not only enhances data augmentation but also accelerates processing through parallel computation. The time series X is segmented into windows $X_w \in \mathbb{R}^{B \times C \times W}$ using a window of length W and stride S , where $w = 1, \dots, n$ represents the window index and n is the total number of windows. Each window X_w is then processed by subsequent attention and temporal convolution blocks. The number of windows n is calculated as:

$$n = \left\lfloor \frac{\text{length} - \text{window_size}}{\text{stride}} \right\rfloor + 1 \quad (8)$$

Here, *length*, *window_size*, and *stride* denote the total length of the time series, the length of each window, and the stride between windows, respectively.

3) *Multi-head Attention Module*: Each subsequence X_w derived from sliding window segmentation is processed as described in (1). The attention context vector c_{ht} for each head is computed as a weighted sum of the values, with weights $\alpha_{htt'}$ determined by the scaled dot-product attention mechanism as (2), and then used in (3).

The context vectors c_{1t}, \dots, c_{Ht} from all heads are concatenated and linearly transformed to yield the final output of the MHA layer:

$$X'_w = W^O[c_{1t}, \dots, c_{Ht}] + X_w, \quad (9)$$

where $W^O \in \mathbb{R}^{d_H \times d}$ is the output projection matrix. This procedure projects the combined outputs back to the original input dimension. Subsequently, X'_w is integrated with the original subsequence X_w through a residual connection and normalized once more. This advanced MHA framework significantly enhances the model's capacity to discern intricate temporal patterns and dependencies within EEG signals, thereby augmenting the precision of decoding activities.

4) *Temporal Convolution*: Following the MHA mechanism, the output X'_w is normalized using *LayerNorm*. The normalized EEG data are denoted as $X_i \in \mathbb{R}^{c \times l}$, where c represents the number of EEG channels and l represents the temporal dimension's sample length.

To extract dynamic temporal features, we employ a temporal convolutional block on each window of the EEG data. The normalized EEG data X_i serves as the input to this block. The temporal convolutional block processes X_i and generates an output tensor $Z_{tcn}^w \in \mathbb{R}^{B \times C \times T_w}$, where T_w represents the window's temporal length and w indexes the window. Batch normalization is applied to the output to ensure training stability, followed by a *ReLU*(\cdot) activation function to introduce non-linearity. The output Z_{tcn}^w is computed as follows:

$$Z_{tcn}^w = \text{ReLU}(\text{BatchNorm}(\text{Conv1d}(X_i))) \quad (10)$$

5) *Feature Fusion*: The outputs of the temporal learner for each window, denoted as $Z_{tcn}^w \in \mathbb{R}^{B \times C \times T_w}$, are assembled into a four-dimensional tensor $Z_{stacked}$:

$$Z_{stacked} = [Z_{tcn}^1, Z_{tcn}^2, \dots, Z_{tcn}^W] \in \mathbb{R}^{B \times C \times W \times T_w} \quad (11)$$

This tensor is rearranged and flattened to meet the convolution layer's input requirements, resulting in dimensions $(B, 32, -1)$, where 32 is the fixed channel count, and -1 represents the flattened dimensions. A fusion convolution layer with a kernel size of 3 and a stride of 1 integrates the outputs across all windows. The final output $Z_{fused} \in \mathbb{R}^{B \times 32 \times L}$, where L is the combined length, captures global contextual information, allowing for a more discriminative representation of features in EEG signals, which is crucial for constructing nodes in GNNs.

C. Graph-based Learning

1) *Graph Filtering Layer*: For the extracted features, we adopt the method described by [16], which involves defining functional areas and performing local filtering. The electrodes are divided into three functional areas: the general region (G_g), the frontal region (G_f), and the hemispheric region (G_h), as shown in Fig. 2. Each channel is treated as a node, and the learned dynamic temporal representations are considered as node attributes.

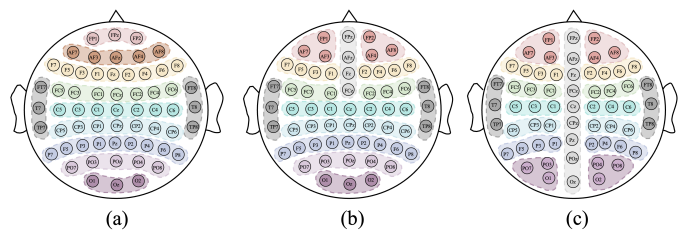


Fig. 2: Local global graph definitions [16]. (a) General definition G_g . (b) Frontal definition G_f . (c) Hemispheric definition G_h .

In the preprocessing step, EEG channels are systematically reordered within predefined groups to ensure adjacency of

channels within each local graph. This reordering enhances the effectiveness of localized graph-based operations applied in subsequent stages. Mathematically, the reordering of channel representations, denoted by $Z_{reorder}^i$, is defined by the function $F_{reorder}(\cdot)$, which operates on the fused data from EEG channels at the i -th observation representations Z_{fuse}^i . This relationship is expressed as:

$$Z_{reorder}^i = F_{reorder}(Z_{fuse}^i) \quad (12)$$

After reordering, a graph filtering layer is employed to aggregate the transformed representations of EEG channels using a fully connected local adjacency matrix A_{local} , where all elements are set to 1. The filtered output $Z_{filtered}^i$ is obtained by applying a trainable filter matrix W_{local} and a bias b_{local} to the reordered data, followed by the application of the $ReLU(\cdot)$ activation function:

$$Z_{filtered}^i = ReLU(W_{local} \circ Z_{reorder}^i + b_{local}) \quad (13)$$

The element-wise product symbol \circ captures localized interactions within the brain.

The output of the filtering process, Z_{local}^i , is aggregated to form localized feature representations using the aggregation function $F_{aggregate}(\cdot)$. The vector representation for each local graph is:

$$Z_{local}^i = F_{aggregate}(Z_{filtered}^i) = \begin{bmatrix} h_{local}^1 \\ \vdots \\ h_{local}^R \end{bmatrix} \quad (14)$$

where $h_{local}^1, \dots, h_{local}^R$ are elements of the localized feature representation vector. These features Z_{local}^i are used to construct the overall feature matrix Z_{agg} :

$$Z_{agg} = \begin{bmatrix} Z_{local}^1 \\ Z_{local}^2 \\ \vdots \\ Z_{local}^{11} \end{bmatrix} \quad (15)$$

2) *Stacked DGNN*: We introduce a stacked DGNN architecture to discern complex structural relationships within graphs. Each layer adaptively recalculates the adjacency matrix based on input features, effectively capturing hierarchical feature variations.

The architecture incorporates multiple GNN layers. In each layer, features are grouped and aggregated into matrices, resulting in an aggregated feature matrix Z_{agg} . The adjacency matrix for each layer is dynamically computed based on the feature similarity matrix S :

$$S = Z_{agg} \cdot Z_{agg}^T \quad (16)$$

Self-loops are introduced by adding the identity matrix I to S , and the modified adjacency matrix A is normalized as:

$$A = S + I, \quad \tilde{A} = \tilde{D}^{-0.5} \cdot A \cdot \tilde{D}^{-0.5} \quad (17)$$

Here, \tilde{D} is the diagonal degree matrix of A , with each diagonal element \tilde{D}_{ii} being the sum of the i -th row of A .

Algorithm 1 AT-DGNN

```

1: Input: EEG data  $X_i \in \mathbb{R}^{E \times T}$ , ground truth label  $y$ 
2: Output:  $pred$ , the prediction of AT-DGNN
3: Initialization; ▷ Feature Extraction
4: for  $i \leftarrow 1$  to  $3$  do
5:   get  $i$ th temporal kernel size by (5);
6:   get  $Z_{temp}^i$  by (6) using  $X_i$  as input;
7: end for
8: get  $Z_T$  by (7);
9: get the window size  $n$  and segment the data by (8);
10: for  $w \leftarrow 1$  to  $n$  do
11:   get window  $X_w \in \mathbb{R}^{B \times E \times W}$ ;
12:   normalize  $X_w$  using LayerNorm;
13:   process  $X_w$  with MHA to get  $X'_w$  by (9);
14:   normalize  $X'_w$  using LayerNorm;
15:   apply TCN on  $X'_w$  to get  $Z_{tcn}^w$  by (10);
16:   add  $Z_{tcn}^w$  to  $Z_{stacked}$ ;
17: end for
18: apply Fusion Conv to  $Z_{stacked}$  to get  $Z_{fused}$  by (11); ▷ Graph-based Learning
19: do graph filtering and aggregation on each node by (12)
- 15 to get  $Z_{local}^i$ ;
20: for  $i \leftarrow 1$  to  $3$  do
21:   get DGNN output by (18);
22: end for
23: get  $pred$  by (19);
24: Return  $pred$ 

```

During forward propagation, each DGNN layer processes the inputs using a normalized adjacency matrix \tilde{A}_i , a weight matrix W_i , and a bias vector b_i for graph convolution. The outputs for each layer are calculated as:

$$\begin{cases} H_1 = ReLU(\tilde{A}_1 \cdot Z_{agg} \cdot W_1 + b_1) \\ H_i = ReLU(\tilde{A}_i \cdot H_{i-1} \cdot W_i + b_i), \quad i \in [2, n-1] \\ H_n = ReLU(\tilde{A}_n \cdot H_{n-1} \cdot W_n + b_n) \end{cases} \quad (18)$$

Here, n denotes the total number of layers in the DGNN, which is set to 3 in our study.

The final *Output* is computed through a sequence of operations including batch normalization $\mathcal{F}_{bn}(\cdot)$, dropout $\mathcal{F}_{dropout}(\cdot)$, and softmax activation $\Phi_{softmax}(\cdot)$, structured as:

$$Output = \Phi_{softmax}(\mathcal{F}_{dropout}(\Gamma(\mathcal{F}_{bn}(H^{(L)})))) \quad (19)$$

where $\Gamma(\cdot)$ denotes the flattening operation, ensuring that the network output is appropriately structured for subsequent processing or analysis.

Finally, the procedure of AT-DGNN can be summarized in Algorithm 1.

IV. EXPERIMENTS

A. MEEG Dataset

In studies on emotion induction, visual stimuli such as images, videos, and text are commonly employed in exper-

iments. However, participants' responses to these stimuli may be influenced by their cultural backgrounds [26]. Considering that the auditory cortex exhibits emotion-specific functional connections with a wide array of limbic, paralimbic, and neocortical structures, suggesting a more extensive role in emotion processing than previously understood [27], we opted to induce emotions in participants using music in the MEEG dataset. We carefully selected 20 music clips, each lasting one minute, characterized by distinct arousal and valence levels, decidedly non-neutral. To minimize emotional carryover, a 15-second pause was introduced between clips [28]. The chosen music pieces included lesser-known works of Western classical music by composers such as Shostakovich and Tchaikovsky. The study involved 32 students from Shandong University, aged between 20 and 25 years, who had no formal music education and were unfamiliar with Western classical music. Each participant signed an informed consent form prior to the study. This experimental design aimed to minimize the influence of social and cultural backgrounds on emotional responses, ensuring that changes in emotions were solely due to musical stimuli, thereby enhancing the accuracy of the experimental results. EEG data were collected using a 32-channel BCI device NeuSen.W32 from Neuracle Tech, employing the same electrode channels as in the DEAP dataset [7]. The data were sampled at a frequency of 1000 Hz. The EEG data were annotated based on the arousal and valence of the music during various stages of the experiment.

B. Experiment Settings

To rigorously evaluate the model's performance, a nested cross-validation approach is employed, featuring a trial-wise 10-fold cross-validation in the outer loop and a 4-fold cross-validation in the inner loop, as suggested by Varma [29]. This stratified sampling technique ensures robustness and generalization of the model by assessing its accuracy and reliability across diverse samples.

Additionally, a two-stage training strategy within the inner loop optimizes the utilization of training data. Initially, the best model identified from the k -fold cross-validation is saved as a preliminary candidate. This model is then refined using combined training data from the k folds, fine-tuned at a reduced learning rate to prevent overfitting, and further trained for up to 20 epochs or until it achieves a training accuracy of 100%, ensuring precise calibration. Importantly, test data is excluded from the training process to maintain the integrity of the evaluation.

The integration of two-stage training with 10-fold cross-validation minimizes variability in assessment results, providing a comprehensive and reliable evaluation framework suitable for diverse research and application domains.

C. Implement Details

The model was implemented using PyTorch [30] library, and the code can be found at <https://github.com/xmh1011/AT-DGNN>.

Cross-entropy loss was chosen as the objective function to guide the training process. The training was divided into two stages, with the first stage capped at 200 epochs and the second at 20 epochs. The batch size was set to 64. To reduce training time and prevent overfitting, early stopping was implemented. For the attention module, the window size was set to half the data frequency. The kernel sizes for the time learner were set to 100, 50, and 25. The hidden layer count for the DGNN was established at 32. Training was optimized using the Adam optimizer, starting with an initial learning rate of $1e-3$, which was reduced by a factor of 10 during the second stage. For more details, please refer to the open-source GitHub repository for AT-DGNN.

V. RESULTS AND DISCUSSION

In this section, we compare the average ACC and F1 score of AT-DGNN on the MEEG dataset with CNN, TCN, and GNN-based SOTA methods in the BCI domain. The CNN-based methods include: EEGNet [9], TSception [24], DeepConvNet and ShallowConvNet [10]. The TCN-based methods include: EEG-TCNet [11], TCNet-Fusion [12] and ATCNet [31]. The GNN-based methods include: DGCNN [18] and LGGNet [16]. Due to the smaller size of the CNN-based models, the learning rate and the number of training epochs are reduced to avoid overfitting. For the other models, the parameters recommended by the authors are used. Additionally, ablation studies are conducted to reveal the contribution of each component within the AT-DGNN architecture.

A. Emotion Recognition

As shown in Table I, the AT-DGNN series, particularly the AT-DGNN-Gen model, significantly outperforms the previous SOTA LGGNet series in both arousal and valence dimensions, with a notable increase in F1 scores and accuracy. The AT-DGNN-Gen model not only achieves the highest accuracy of 83.74% in the arousal dimension, surpassing the LGGNet-Gen model by 1.59%, but also records the highest accuracy of 86.01% in the valence dimension, a substantial improvement of 3.48% over the LGGNet series. This improvement underscores the efficacy of our approach in capturing complex patterns within the MEEG dataset, which is known for its challenging and class-imbalanced nature.

The AT-DGNN-Gen model exemplifies the superior performance of the AT-DGNN series, achieving robust results with an average accuracy of 84.88% and an F1 score of 85.12% across emotion dimensions. This underscores the effectiveness of our graph-based approach in handling complex emotion recognition tasks. Furthermore, consistent with the findings of [16], the graph configuration G_g demonstrated superior performance in both AT-DGNN and LGGNet models compared to other graph definitions, indicating its optimal structure for capturing relevant features in emotion analysis.

Furthermore, these results demonstrate a marked improvement over traditional CNN and TCN-based methods, with average gains in F1 scores and accuracy surpassing previous

TABLE I
COMPARISON OF ACC AND F1 SCORES (MEAN \pm STD) FOR THE MEEG DATASET UNDER TRIAL-WISE 10-FOLD CROSS-VALIDATION

Method	Arousal				Valence				Emotion	
	ACC (%)	std (%)	F1 (%)	std (%)	ACC (%)	std (%)	F1 (%)	std (%)	ACC (%)	F1 (%)
EEGNet	75.47	17.63	75.54	17.83	73.66	16.82	73.33	16.94	74.57	74.44
DeepConvNet	79.35	15.03	78.43	18.10	72.38	18.87	73.03	19.27	75.87	75.73
ShallowConvNet	80.96	14.49	80.87	14.71	79.77	16.44	80.22	15.60	80.37	80.55
TSception	79.23	11.51	81.30	9.84	78.34	15.03	81.18	12.08	78.79	81.24
EEG-TCNet	76.36	17.05	73.79	19.66	69.72	16.06	54.28	22.43	73.04	64.04
TCNet-Fusion	76.72	17.32	76.95	17.49	75.88	16.70	75.42	16.97	76.30	76.20
ATCNet	82.01	14.06	79.17	17.57	83.19	12.09	82.08	13.41	82.60	80.63
DGCNN	82.12	12.05	81.83	12.45	82.72	11.00	82.40	11.44	82.42	82.12
LGGNet-Fro	81.85	12.57	81.58	12.73	82.34	12.84	81.66	13.91	82.11	81.62
LGGNet-Gen	82.15	12.72	82.15	12.57	82.53	13.20	82.47	13.22	82.34	82.31
LGGNet-Hem	81.92	12.08	81.58	12.43	82.37	12.71	81.58	14.13	82.15	81.58
AT-DGNN-Fro	83.51	11.09	83.06	11.83	85.56	10.69	85.61	10.89	84.54	84.34
AT-DGNN-Gen	83.74	12.03	84.56	10.88	86.01	9.40	85.68	10.06	84.88	85.12
AT-DGNN-Hem	83.73	11.20	84.78	10.93	84.89	10.57	85.35	10.24	84.31	85.07

Emotion averages the ACC and F1 scores of both the arousal and valence dimensions.

The results for all models are derived from the optimal values among ten trials with distinct random seeds.

models by up to 7.16% and 5.78%, respectively. This emphasizes the advanced capability of the DGNN approach in graph-structured data analysis, providing more accurate and reliable emotion recognition.

All methods achieve high accuracy on the MEEG dataset, with CNN and TCN models reaching 75% or higher, and GNN models exceeding 80%. On the DEAP dataset, AT-DGNN averages 60.56% accuracy across four dimensions. According to Huang et al. [32], other models, including LGGNet, also achieve around 60% accuracy on DEAP, with some slightly outperforming AT-DGNN and others not. All models perform significantly better on the MEEG dataset, suggesting that music is more effective than video in evoking emotions.

B. Ablation Study

TABLE II
ABLATION STUDY ON EMOTION OF MEEG USING AT-DGNN-GEN.

S	M	D	ACC(%)	Changes(%)	F1(%)	Changes(%)
✓	✓	X	81.91	-2.97	81.81	-3.31
✓	X	3	78.31	-6.57	79.46	-5.66
X	✓	3	80.89	-3.99	81.16	-3.96
✓	✓	I	81.91	-2.97	81.81	-3.31
✓	✓	2	82.94	-1.94	82.52	-2.60
✓	✓	4	83.17	-1.71	83.48	-1.64
✓	✓	3	84.88	-	85.12	-

S: Sliding window segmentation.

M: Multi-head attention mechanism.

D: Dynamic graph neural network.

✓: Keep the component.

X: Exclude the component.

I, **2**, **3**, **4**: The number of stacked DGNN layers.

Changes: Compared with the baseline AT-DGNN-Gen.

As illustrated in Table II, an ablation study is conducted to systematically assess the individual contributions of critical components within the AT-DGNN model: sliding window

segmentation (S), multi-head attention mechanism (M), and the dynamic graph neural network (D). The results underscore the pivotal roles of these components, indicating that their omission results in declines in accuracy (ACC) of 2.97%, 6.57%, and 3.99% and in F1 scores of 3.31%, 5.66%, and 3.96%, respectively, thereby demonstrating their functionality and synergy.

Furthermore, the experiment demonstrated that the number of layers in the DGNN significantly affects the model's performance. Modifying the number of DGNN layers to 1, 2, or 4 led to reductions in accuracy of 2.97%, 1.94%, and 1.71%, and in F1 scores of 3.31%, 2.60%, and 1.64%, respectively. A configuration with a single layer implies non-utilization of the stacked DGNN, highlighting the importance of network depth tuning in optimizing the model's capacity to process and analyze complex relationships in EEG data.

The optimal configuration, employing 3 layers of the DGNN, is found to be the most effective, as evidenced by achieving the highest scores in both ACC and F1 metrics. These findings substantiate the design choices of the AT-DGNN model and shed light on the interaction among its components, significantly enhancing computational neuroscience analysis.

VI. CONCLUSION

This study introduces the MEEG dataset and the AT-DGNN framework, marking substantial progress in the field of EEG-based emotion recognition. The MEEG dataset uniquely employs music to induce emotional states, providing an invaluable resource for probing brain responses to emotional stimuli. The AT-DGNN, which integrates attention mechanisms with DGNN, adeptly captures the intricate temporal dynamics of brain activity, thereby markedly enhancing emotion recognition accuracy over existing SOTA methods. This advancement not only propels BCI technology forward but also facilitates novel investigations into the interplay among music,

emotion, and cerebral activity. The exemplary performance of AT-DGNN, validated through rigorous comparisons with traditional models, solidifies its utility in advancing neuropsychological understanding.

REFERENCES

- [1] S. Schachter and J. Singer, “Cognitive, social, and physiological determinants of emotional state.” *Psychological review*, vol. 69, no. 5, p. 379, 1962.
- [2] J. A. Russell, “A circumplex model of affect.” *Journal of personality and social psychology*, vol. 39, no. 6, p. 1161, 1980.
- [3] G. Schalk, D. J. McFarland, T. Hinterberger, N. Birbaumer, and J. R. Wolpaw, “Bci2000: a general-purpose brain-computer interface (bci) system,” *IEEE Transactions on biomedical engineering*, vol. 51, no. 6, pp. 1034–1043, 2004.
- [4] S. Zhao, G. Jia, J. Yang, G. Ding, and K. Keutzer, “Emotion recognition from multiple modalities: Fundamentals and methodologies,” *IEEE Signal Processing Magazine*, vol. 38, no. 6, pp. 59–73, 2021.
- [5] T. Mushi, Y. Terasaki, H. A. Haque, and G. A. Ivamitsky, “Feature extraction from eegs associated with emotions,” *Artificial Life and Robotics*, vol. 1, no. 1, pp. 15–19, 1997.
- [6] R. Foong, K. K. Ang, C. Quek, C. Guan, K. S. Phua, C. W. K. Kuah, V. A. Deshmukh, L. H. L. Yam, D. K. Rajeswaran, N. Tang *et al.*, “Assessment of the efficacy of eeg-based mibci with visual feedback and eeg correlates of mental fatigue for upper-limb stroke rehabilitation,” *IEEE Transactions on Biomedical Engineering*, vol. 67, no. 3, pp. 786–795, 2019.
- [7] S. Koelstra, C. Muhl, M. Soleymani, J.-S. Lee, A. Yazdani, T. Ebrahimi, T. Pun, A. Nijholt, and I. Patras, “Deap: A database for emotion analysis; using physiological signals,” *IEEE transactions on affective computing*, vol. 3, no. 1, pp. 18–31, 2011.
- [8] W.-L. Zheng and B.-L. Lu, “Investigating critical frequency bands and channels for eeg-based emotion recognition with deep neural networks,” *IEEE Transactions on autonomous mental development*, vol. 7, no. 3, pp. 162–175, 2015.
- [9] V. J. Lawhern, A. J. Solon, N. R. Waytowich, S. M. Gordon, C. P. Hung, and B. J. Lance, “Eegnet: a compact convolutional neural network for eeg-based brain–computer interfaces,” *Journal of neural engineering*, vol. 15, no. 5, p. 056013, 2018.
- [10] R. T. Schirrmeister, J. T. Springenberg, L. D. J. Fiederer, M. Glasstetter, K. Eggensperger, M. Tangermann, F. Hutter, W. Burgard, and T. Ball, “Deep learning with convolutional neural networks for eeg decoding and visualization,” *Human brain mapping*, vol. 38, no. 11, pp. 5391–5420, 2017.
- [11] T. M. Ingolfsson, M. Hersche, X. Wang, N. Kobayashi, L. Cavigelli, and L. Benini, “Eeg-tcnet: An accurate temporal convolutional network for embedded motor-imagery brain–machine interfaces,” in *2020 IEEE International Conference on Systems, Man, and Cybernetics (SMC)*. IEEE, 2020, pp. 2958–2965.
- [12] Y. K. Musallam, N. I. AlFassam, G. Muhammad, S. U. Amin, M. Alsulaiman, W. Abdul, H. Altaheri, M. A. Bencherif, and M. Algabri, “Electroencephalography-based motor imagery classification using temporal convolutional network fusion,” *Biomedical Signal Processing and Control*, vol. 69, p. 102826, 2021.
- [13] Y. S. Can, B. Mahesh, and E. André, “Approaches, applications, and challenges in physiological emotion recognition—a tutorial overview,” *Proceedings of the IEEE*, 2023.
- [14] M. Graña and I. Morais-Quilez, “A review of graph neural networks for electroencephalography data analysis,” *Neurocomputing*, p. 126901, 2023.
- [15] N. Robinson, S.-W. Lee, and C. Guan, “Eeg representation in deep convolutional neural networks for classification of motor imagery,” in *2019 IEEE International Conference on Systems, Man and Cybernetics (SMC)*. IEEE, 2019, pp. 1322–1326.
- [16] Y. Ding, N. Robinson, C. Tong, Q. Zeng, and C. Guan, “Lggnnet: Learning from local-global-graph representations for brain–computer interface,” *IEEE Transactions on Neural Networks and Learning Systems*, 2023.
- [17] F. Scarselli, M. Gori, A. C. Tsoi, M. Hagenbuchner, and G. Monfardini, “The graph neural network model,” *IEEE transactions on neural networks*, vol. 20, no. 1, pp. 61–80, 2008.
- [18] T. Song, W. Zheng, P. Song, and Z. Cui, “Eeg emotion recognition using dynamical graph convolutional neural networks,” *IEEE Transactions on Affective Computing*, vol. 11, no. 3, pp. 532–541, 2018.
- [19] G. Bao, K. Yang, L. Tong, J. Shu, R. Zhang, L. Wang, B. Yan, and Y. Zeng, “Linking multi-layer dynamical gcn with style-based recalibration cnn for eeg-based emotion recognition,” *Frontiers in Neurorobotics*, vol. 16, p. 834952, 2022.
- [20] S. Asadzadeh, T. Yousefi Rezaii, S. Beheshti, and S. Meshgini, “Accurate emotion recognition using bayesian model based eeg sources as dynamic graph convolutional neural network nodes,” *Scientific Reports*, vol. 12, no. 1, p. 10282, 2022.
- [21] H. Zhao, J. Liu, Z. Shen, and J. Yan, “Scc-mpgen: self-attention coherence clustering based on multi-pooling graph convolutional network for eeg emotion recognition,” *Journal of Neural Engineering*, vol. 19, no. 2, p. 026051, 2022.
- [22] J. Zhang, X. Zhang, G. Chen, and Q. Zhao, “Granger-causality-based multi-frequency band eeg graph feature extraction and fusion for emotion recognition,” *Brain Sciences*, vol. 12, no. 12, p. 1649, 2022.
- [23] A. Pedroni, A. Bahreini, and N. Langer, “Automatic: Standardized preprocessing of big eeg data,” *NeuroImage*, vol. 200, pp. 460–473, 2019.
- [24] Y. Ding, N. Robinson, Q. Zeng, D. Chen, A. A. P. Wai, T.-S. Lee, and C. Guan, “Tception: a deep learning framework for emotion detection using eeg,” in *2020 international joint conference on neural networks (IJCNN)*. IEEE, 2020, pp. 1–7.
- [25] Robin, Tibor, Schirrmeister, Jost, Tobias, Springenberg, Lukas, Dominique, Josef, and Fiederer, “Deep learning with convolutional neural networks for eeg decoding and visualization.” *Human Brain Mapping*, 2017.
- [26] P. N. Juslin and D. Västfjäll, “Emotional responses to music: The need to consider underlying mechanisms,” *Behavioral and brain sciences*, vol. 31, no. 5, pp. 559–575, 2008.
- [27] S. Koelsch, “Brain correlates of music-evoked emotions,” *Nature reviews neuroscience*, vol. 15, no. 3, pp. 170–180, 2014.
- [28] S. Sheykhiand, Z. Mousavi, T. Y. Rezaii, and A. Farzamnia, “Recognizing emotions evoked by music using cnn-lstm networks on eeg signals,” *IEEE Access*, vol. PP, no. 99, pp. 1–1, 2020.
- [29] S. Varma and R. Simon, “Bias in error estimation when using cross-validation for model selection,” *BMC bioinformatics*, vol. 7, pp. 1–8, 2006.
- [30] A. Paszke, S. Gross, F. Massa, A. Lerer, J. Bradbury, G. Chanan, T. Killeen, Z. Lin, N. Gimelshein, L. Antiga *et al.*, “Pytorch: An imperative style, high-performance deep learning library,” *Advances in neural information processing systems*, vol. 32, 2019.
- [31] H. Altaheri, G. Muhammad, and M. Alsulaiman, “Physics-informed attention temporal convolutional network for eeg-based motor imagery classification,” *IEEE transactions on industrial informatics*, vol. 19, no. 2, pp. 2249–2258, 2022.
- [32] Y.-C. Huang, Y. Lu, X.-Y. Si, J. Yang, S.-M. Zhou, and Y. Yan, “Mt-lgsgcn: Eeg-based emotion recognition using multi-scale temporal and local-global spatial graph convolution network,” in *2023 IEEE International Conference on Bioinformatics and Biomedicine (BIBM)*. IEEE, 2023, pp. 2632–2638.